Kinetics of the OH + ClOOCl and OH + Cl_2O Reactions: Experiment and Theory†

Jaron C. Hansen,‡,* Randall R. Friedl, and Stanley P. Sander

Jet Propulsion Laboratory, California Institute of Technology, Pasadena, California 91109

Received: January 25, 2008; Revised Manuscript Received: June 9, 2008

The rate coefficients for the reactions OH + ClOOCl → HOCl + ClOO (eq 5) and OH + Cl_2O → HOCl + ClO (eq 6) were measured using a fast flow reactor coupled with molecular beam quadrupole mass spectrometry. OH was detected using resonance fluorescence at 309 nm. The measured Arrhenius expressions for these reactions are $k_5 = (6.0 \pm 3.5) \times 10^{-13} \exp((670 \pm 230)/T)$ cm^3 molecule^{-1} s^{-1} and $k_6 = (5.1 \pm 1.5) \times 10^{-12} \exp((100 \pm 92)/T)$ cm^3 molecule^{-1} s^{-1}, respectively, where the uncertainties are reported at the 2σ level. Investigation of the OH + ClOOCl potential energy surface using high level ab initio calculations indicates that the reaction occurs via a chlorine abstraction from ClOOCl by the OH radical. The lowest energy pathway is calculated to proceed through a weak ClOOCl−OH prereactive complex that is bound by 2.6 kcal mol^{-1} and leads to ClOO and HOCl products. The transition state to product formation is calculated to be 0.59 kcal mol^{-1} above the reactant energy level. Inclusion of the OH + ClOOCl rate data into an atmospheric model indicates that this reaction contributes more than 15% to ClOOCl loss during twilight conditions in the Arctic stratosphere. Reducing the rate of ClOOCl photolysis, as indicated by a recent re-examination of the ClOOCl UV absorption spectrum, increases the contribution of the OH + ClOOCl reaction to polar stratospheric loss of ClOOCl.

Introduction

Recent aircraft measurements of ClO and ClOOCl ("ClO dimer") by Stimpfle et al.[1] in the Arctic polar vortex have focused attention on the role of these species in the catalytic destruction of stratospheric ozone:

$$\mathrm{ClO + ClO + M \rightarrow ClOOCl + M} \quad (1)$$

$$\mathrm{ClOOCl + h\nu \rightarrow Cl + ClOO} \quad (2)$$

$$\mathrm{ClOO + M \rightarrow Cl + O_2 + M} \quad (3)$$

$$\frac{2(\mathrm{Cl + O_3 \rightarrow ClO + O_2})}{\text{Net: } 2\mathrm{O_3 \rightarrow 3O_2}} \quad (4)$$

This study found that the measured ClOOCl concentrations were inconsistent with the predictions of a photochemical model that used rate parameters for ClOOCl formation, photolysis, and thermal decomposition derived from the most recent NASA recommendations.[2] For daytime observations, agreement could only be obtained by decreasing the formation rate or increasing the photolysis rate in the model between 25 and 40%. For nighttime observations, agreement was obtained only by decreasing the formation rate or increasing the thermal decomposition rate by approximately a factor of 2. Adding to the uncertainty is a recent laboratory study that showed that ClOOCl photolysis in the near-UV is slower than previously thought. Using improved methods for the synthesis and purification of ClOOCl, Pope et al.[3] measured cross sections at wavelengths longer than 300 nm that result in photolysis rates that are a factor of six smaller than the NASA-recommended values. This large discrepancy calls into question the completeness of present atmospheric models of polar ozone depletion and raises questions about other possible removal mechanisms for ClOOCl.

The discrepancy between modeled and observed ClOOCl concentrations might be explained if there are atmospheric loss processes that are not in the standard models. Reactions of ClOOCl with Cl and Br atoms have been shown to be relatively rapid; however, the small atom abundances ($< 10^6$ cm^{-3}) in the lower polar stratosphere preclude a significant role for these reactions. (Ingham et al.,[4] Cox et al.[5,6]) Another possibility is reaction of ClOOCl with the OH radical, which is present in significantly higher abundance in the polar stratosphere ($> 10^6$ cm^{-3}).

$$\mathrm{OH + ClOOCl \rightarrow HOCl + ClOO} \quad (5)$$

At the present time, no measurements of the rate coefficients for reaction 5 exist. However, measurements have been reported by Stevens et al.[7] for the analogous Cl_2O + OH reaction (eq 6).

$$\mathrm{OH + Cl_2O \rightarrow HOCl + ClO} \quad (6)$$

Noting the similarity between rate coefficients for Cl_2O and ClOOCl reactions with Br and Cl atoms, Stevens et al.[7] suggested that the rate constant for reaction of OH with ClOOCl may be as large as that for OH + Cl_2O. They also suggested that the ClOOCl reaction, like that of Cl_2O, will likely involve formation of a stable intermediate and will exhibit a negative temperature dependence. These suggestions carry potentially important implications for polar stratospheric ozone processes. As pointed out by Stevens et al.,[7] a fast rate for reaction 5 would shift the catalytic destruction for ozone from one involving ClO dimer photolysis to one involving HOCl photolysis.

$$\mathrm{ClO + ClO + M \rightarrow ClOOCl + M} \quad (1)$$

$$\mathrm{OH + ClOOCl \rightarrow HOCl + ClOO} \quad (5)$$

$$\mathrm{ClOO + M \rightarrow Cl + O_2 + M} \quad (3)$$

$$\mathrm{HOCl + h\nu \rightarrow OH + Cl} \quad (7)$$

* Corresponding author. E-mail: jhansen@chem.byu.edu. Fax: (801) 422-0153. Phone: (801) 422-4066.

† Part of the "Stephen R. Leone Festschrift."

‡ Present address: Department of Chemistry and Biochemistry, Brigham Young University, Provo, Utah 84602.

10.1021/jp8007706 CCC: $40.75
Published on Web 08/15/2008

$$\frac{2(Cl + O_3 \rightarrow ClO + O_2)}{\text{Net: } 2O_3 \rightarrow 3O_2} \quad (4)$$

To determine the importance of reaction 5 among the reactions controlling the production and removal of ClOOCl and its role in the catalytic destruction of stratospheric ozone, we have investigated the kinetics of this reaction using a fast flow reactor coupled with mass spectrometric and resonance fluorescence detection. To better understand the reaction mechanism, we have calculated the structures and energies of key intermediates on the potential energy surface for reaction 5. We have also measured temperature-dependent rate constants for the closely related OH + Cl_2O reaction.

Experimental Method

Discharge Flow Reactor. A discharge flow reactor coupled with resonance fluorescence and mass spectrometric detection was used to probe the kinetics of the OH + Cl_2O and OH + ClOOCl reactions as depicted in Figure 1. The main reactor consisted of a 90 cm-long, 3.6 cm-i.d. Pyrex tube coated with halocarbon wax (halocarbon 1500) to reduce wall loss. The reactor temperature, as measured with a thermocouple located inside the outer jacket, was varied between 223 and 318 K by circulation of either cooled methanol or heated water through an outer jacket of the reactor. Temperature gradients inside the reactor were measured by inserting a thermocouple into the reactor with the gases flowing. Axial temperature gradients were less than 2 °C between the ends of the 60 cm reaction zone for all experimental temperatures. The reported temperature for each kinetic trial represents the average axial temperatures measured in the reaction zone.

A total pressure of approximately 1 Torr was maintained in the reactor by flowing between 800 and 1200 sccm of carrier gas into the main reactor. The flowing gases were pumped out of the reactor through a throttle valve and liquid nitrogen trap by a 100 cfm mechanical pump (Welch 1396). Helium was the main carrier gas and was admitted through sidearm ports into the reactor. Flow velocities ranged between 700 and 1200 cm s^{-1}. The reaction times could be varied between 16 and 97 ms by moving the sliding injector. The reactor walls were passivated for approximately 2 h before each kinetic run by flowing both OH and ClOOCl or Cl_2O through the reactor at the selected temperature.

Kinetic runs were performed under pseudo first-order conditions, with either Cl_2O or ClOOCl in excess over OH radicals. The reactants were added to the reactor through either a fixed sidearm port upstream of the reaction zone or through a 180 cm long, 0.6 cm i.d. Pyrex sliding injector that was concentric with the main flow tube. Both the inside and outside surfaces of the sliding injector were coated with halocarbon wax to inhibit OH and ClOOCl (or Cl_2O) wall losses, respectively. Movement of the sliding injector varied the contact time between the excess reagent and the OH radical. Typically, six different positions (distances) of the sliding injector were used to characterize a particular OH decay.

For the OH + Cl_2O reaction, runs were first conducted by injecting Cl_2O through the sliding injector and OH through the fixed sidearm. A second set of runs was conducted with the sources reversed. For the OH + ClOOCl reaction, runs were only carried out with ClOOCl added through the fixed sidearm due to the relatively large ClOOCl losses observed inside the sliding injector. The observed OH decays were corrected for axial diffusion and wall loss according to the following equation,

$$k_{corr} = k'(1 + k'D/v^2) - k_w \quad \text{(eq1)}$$

where k_{corr} is the corrected first order rate constant, D is the diffusion coefficient for the OH radical in 1 Torr He, v is the mean bulk flow velocity, k_w is the first order rate of OH loss on the walls of the main reactor or injector (depending on source configuration), and k' is the observed OH pseudo first-order decay constant. The diffusion coefficient for OH radical in He was estimated from the data of Marrero and Mason.[8] Values of D ranged from 0.64 $cm^2\ s^{-1}$ at 223 K to 1.08 $cm^2\ s^{-1}$ at 318 K. The correction for axial diffusion never exceeded 4% of the observed OH decays (k').

Values for k_w were measured at the beginning and end of each kinetic run and were essentially constant. OH wall loss generally increased with decreasing temperature, ranging between 2−5 s^{-1} at 298 K and 15−25 s^{-1} at 223 K. On account of the large loss rates at low temperatures, we limited our experiments to temperatures no lower than 223 K.

The bimolecular rate constants (k) were obtained from the slopes of weighted ($1/\sigma^2$ with σ representing the combination of random and estimated systematic errors) linear least-squares fits of plots of k_{corr} versus excess reactant concentration. The reaction activation barrier (E_a) and Arrhenius (A) factor for the reaction of OH radical with ClOOCl were determined from the slopes and intercepts of weighted plots of the natural logarithm of k versus $1/T$.

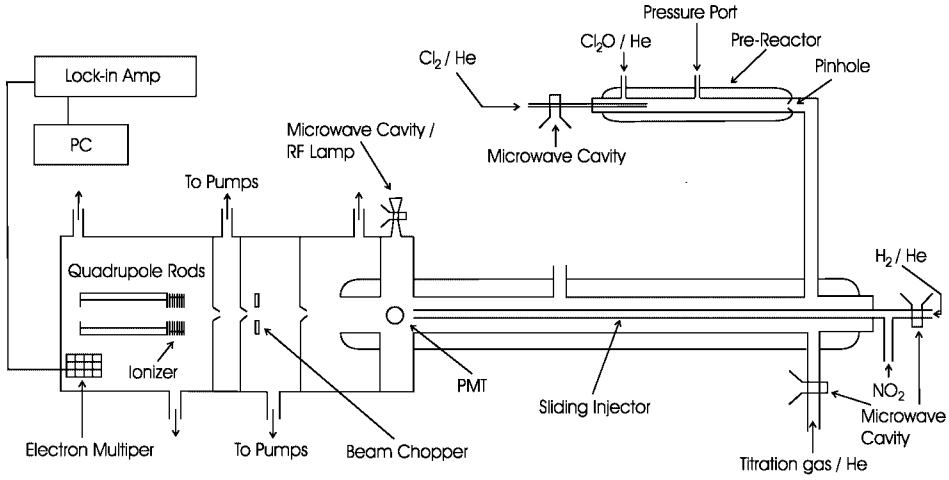

Figure 1. Schematic of the discharge flow/resonance fluorescence/mass spectrometer.

For rate constant determinations, pressure measurements were made with capacitance manometers calibrated against a secondary standard. Gas flow measurements were made using electronic flow controllers/meters (Hastings), which were calibrated by means of the bubble displacement method. The estimated systematic uncertainties (2σ) in the experimental measurements are as follows: pressure (1%), gas flow rates (5%), and absolute calibration (i.e., response of the mass spectrometer to the excess reagent) of the mass spectrometer (1−12%). These systematic errors were combined in quadrature with the observed random errors to give experimental uncertainties in the derived rate coefficients.

Resonance Fluorescence and Mass Spectrometric Detection. The OH radical was measured by resonance fluorescence, monitoring the $A^2\Sigma^+ - X^2\Pi$ (0,0) electronic transition centered at 309 nm. The light source was an Evenson-type microwave discharge in a H_2O/He mixture (3 Torr, ∼3% H_2O) operating at 70 W. To decrease scattered light from the discharge, the output from the resonance lamp was passed through a two inch stack of baffles (1/2 in. i.d.) and then directed radially through the main reaction cell. Further reduction in the scattered light was obtained by coating the resonance fluorescence reaction zone with carbon-black, to which an overcoat of halocarbon wax was applied.

The scattered fluorescence was detected on a perpendicular axis using a bialkali photomultiplier tube (PMT), (Electron Tubes P25PC) operating in photon counting mode. A 309 ± 4.5 nm band-pass filter (50% transmission at 309 nm, Barr Associates Inc. Model No. 1229813) was placed behind another 2 in. stack of baffles (1/2 in. i.d.) in order to further discriminate against light scattered from the walls.

Reactants (ClOOCl and Cl_2O), products, and other species were quantified using mass spectrometric detection. The mass spectrometer consisted of a three-stage differentially pumped quadrupole mass filter, which utilized electron impact ionization (35 eV) and a channeltron detector.[9,10] A molecular beam was formed by passing the gas flow from the main reactor through a series of coaxial pinholes at the entrance to the differentially pumped chambers. The molecular beam was chopped at 200 Hz with a tuning fork chopper located directly behind the first pinhole. The channeltron anode current was amplified using a lock-in amplifier referenced to the chopper frequency. The amplified analog signals were digitized (Analog Devices RTI/815), recorded, and averaged on a personal computer using software written in Labview.

Reactant Generation. OH was produced by reacting atomic hydrogen with nitrogen dioxide. Hydrogen atoms ($(0.8-3) \times 10^{11}$ atoms cm^{-3}) were generated by discharging 1% H_2/He in an Evenson-type microwave discharge operating at ∼1 Torr and at ∼20 W. The H atoms were titrated with a slight excess of NO_2 ($(1-5) \times 10^{11}$ molecules cm^{-3}) to produce NO and OH radicals. The result was the production of $(0.5-2) \times 10^{11}$ molecules cm^{-3} of OH radical in the main reaction cell. A slight excess of NO_2 was used in order to ensure that no H atoms were introduced into the main reactor cell.

Cl_2O was synthesized by passing a 10% Cl_2/He (∼15 sccm) mixture kept at atmospheric pressure through a U-tube containing glass beads and yellow HgO (Aldrich, 99+%). The reddish-brown Cl_2O eluent was collected at 193 K in a trap cooled by a methanol/dry ice bath. With this procedure, the main impurity was found to be unreacted Cl_2. Purification of Cl_2O was accomplished by extended pumping on the sample at 193 K, where the vapor pressure of Cl_2 (∼50 Torr) is substantially higher that that of Cl_2O (∼6 Torr). The purity of the remaining Cl_2O was checked by UV absorption spectroscopy and was found to be better than 99.8%.[11,12] The effect of the small remaining quantities of Cl_2 on the observed OH decays was negligible (<1 s^{-1}) due to the low Cl_2 + OH reaction rate coefficient.[2]

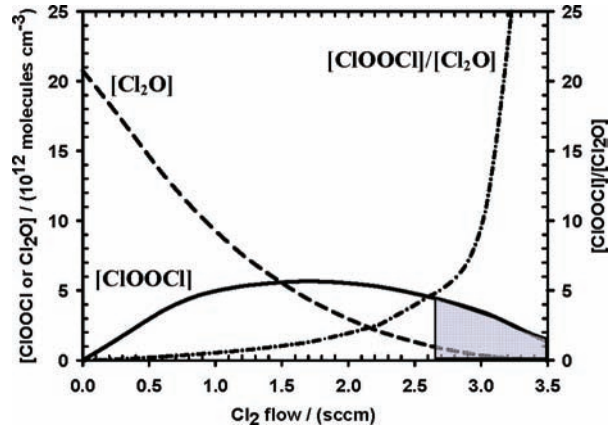

Figure 2. Prereactor output as a function of Cl_2 input flow rate. Dashed line, $[Cl_2O] \times 10^{12}$ molecules cm^{-3}; solid line, $[ClOOCl] \times 10^{12}$ molecules cm^{-3}; dash-dot-dash line, [ClOOCl]/[Cl_2O]; the gray-filled area represents the range of [ClOOCl] used in these experiments.

ClOOCl was generated from the termolecular channel of the ClO self-reaction (reaction 1) inside a 38 cm-long, 2.5 cm-i.d. jacketed prereactor coated with halocarbon wax. The prereactor was separated from the main reactor cell by a pinhole. To promote the formation of ClOOCl, the prereactor was cooled (∼200 K) by the circulation of chilled methanol through an outer jacket (Neslab ULT-80), the pressure was set between 25−30 Torr, and the residence time was maintained at a relatively long ∼3−4 s.

ClO was generated upstream of the prereactor by reacting atomic chorine with Cl_2O.

$$Cl + Cl_2O \rightarrow ClO + Cl_2 \qquad (8)$$

Chlorine atoms were generated by discharging Cl_2 (10%/He) in a Beenakker-type microwave cavity operated at approximately 30 W and located at the upstream end of a 38 cm-long, 0.4 cm-i.d. fixed quartz injector tube. The tube was coated with *o*-phosphoric acid in order to increase the Cl_2 dissociation efficiency by inhibiting the chlorine atom recombination. An excess of Cl_2O ($(0.8-1.7) \times 10^{13}$ molecules cm^{-3} in the prereactor) was used to completely convert chlorine atoms to ClO and Cl_2. This was verified by the observed absence of $BrCl^+$ ($m/z = 116$) in the presence of an added flow of Br_2 to the prereactor. From our observations, we were able to place an upper limit of 2×10^{10} atoms cm^{-3} on the chlorine atom concentration reaching the main reactor.

The concentration of unreacted ClO exiting the prereactor was probed by adding NO to the main flow reactor and detecting the NO_2 product ($m/z = 46$). The highest NO_2 concentration that was observed in the main reactor under the conditions in which kinetic runs were performed for ClOOCl was 8×10^{10} molecules cm^{-3}. With this concentration of ClO, the contribution to the OH decay due to the reaction of ClO with OH is small ($k' \approx 1$ s^{-1}).

Figure 2 shows the loss of Cl_2O and the production of ClOOCl as a function of molecular chlorine flow (sccm) through the microwave discharge (Cl atom production is proportional to the Cl_2 flow). At low Cl_2 flow rates, decreases in Cl_2O are accompanied by increases in ClOOCl (from 0 to 5×10^{12} molecules cm^{-3}), the result of reactions 8 and 1. However,

ClOOCl concentrations remain smaller that those of Cl_2O over this range. Concentrations of ClOOCl do not predominate over those of Cl_2O until both species begin to decrease as a result of increasing loss due to reaction with Cl.

As a consequence of the conditions in the prereactor, the upper limit of [ClOOCl] that could be used in the kinetic studies of OH + ClOOCl was approximately 5×10^{12} molecules cm^{-3}. At these highest ClOOCl levels, up to 25% of the observed OH decay was due to the reaction of residual Cl_2O in the main reactor. Accordingly, it was necessary to correct the observed OH first order decays (k') for loss by Cl_2O. Corrections for Cl_2O at lower concentrations of ClOOCl could be minimized by working at the highest Cl_2 flows. The lowest concentration of ClOOCl used for the kinetic runs was approximately 5×10^{11} molecules cm^{-3} and was determined by the minimum value of k' that could be reliably measured ($\sim 5\ s^{-1}$).

Secondary chemistry arising from the chain reaction of chlorine atoms produced from the reaction of OH with ClOOCl dictated that the reaction be run under conditions of [OH] $\ll$ [ClOOCl] ([OH] $\approx (0.5-2) \times 10^{11}$ molecules cm^{-3})

$$OH + ClOOCl \rightarrow HOCl + ClOO \quad (5b)$$

$$ClOO + M \rightarrow Cl + O_2 + M \quad (3b)$$

$$Cl + ClOOCl \rightarrow Cl_2 + ClOO \quad (9)$$

Additionally, the [ClOOCl] was monitored with the mass spectrometer throughout each kinetic run. The [ClOOCl] was never observed to decrease more than 5% over the duration of the kinetic run.

The laboratory gases used in this study, along with their stated purities, were as follows: He (UPC, 99.9993%, Airgas) for bulk flow and the OH resonance lamp; He (Research grade, 99.9995%, Air Products) the carrier gas for the H_2 discharge; 10% Cl_2/He (Matheson) used for the production of Cl_2O and ClOOCl; 1% H_2/He (Air Liquide) passed through the microwave discharge for the production of OH radicals; NO_2 (Matheson) reacted with H atoms to produce OH radicals; and NO (UHP, 99.999%, Matheson) used in the titration of ClO.

Reactant Calibration. The concentration of OH radicals was determined by titration with Br_2. The loss of Br_2 was detected by observation of Br_2^+ at $m/z = 160$. The sensitivity of OH was found to be approximately 3×10^{-7} counts s^{-1} (molecules $cm^{-3})^{-1}$ with a background of approximately 500 counts s^{-1}, resulting in a detection limit of approximately 2×10^7 molecules cm^{-3} for 20 s averaging.

Cl_2O concentrations in the flow reactor were determined using two different techniques. The first technique involved comparing measured mass spectrometric signals (Cl_2O^+ $m/z = 86$) to measured flows of Cl_2O from "standard" bulbs containing known concentrations of Cl_2O in helium. The standard bulb mixtures were prepared by mixing approximately 8 Torr of purified Cl_2O with 800 Torr of helium. Calibration curves, generated by measuring the ion signal at a series of different Cl_2O flows, were taken at the beginning and end of each series of kinetic runs. Calibration variations never varied by more than 2% over the course of an experiment.

A second calibration technique relied on titration of Cl_2O by Br atoms.

$$Br + Cl_2O \rightarrow BrCl + ClO \quad (10)$$

Bromine atoms were produced by passing molecular bromine ($\sim 1 \times 10^{13}$ molecules cm^{-3}) through an Evenson-type microwave cavity operating at approximately 1 Torr and 50 W. The generated bromine atoms were allowed to react with Cl_2O for approximately 70 ms, resulting in the conversion of Cl_2O into BrCl. The loss of Cl_2O was monitored with respect to the gain in the $BrCl^+$ signal ($m/z = 116$). BrCl ion signals were calibrated by comparing to measured flows of BrCl from standard bulbs. The standard bulbs of BrCl were prepared by mixing an excess of Cl_2 ($\sim$100 Torr) with Br_2 ($\sim$1.5 Torr) in a 4 L Pyrex bulb and allowing the mixture to thermally react for at least two days. The resulting equilibrium mixture of BrCl, Br_2, and Cl_2 greatly favored BrCl relative to Br_2. The partial pressure of BrCl in the mixture was determined from the reported equilibrium constant.[13]

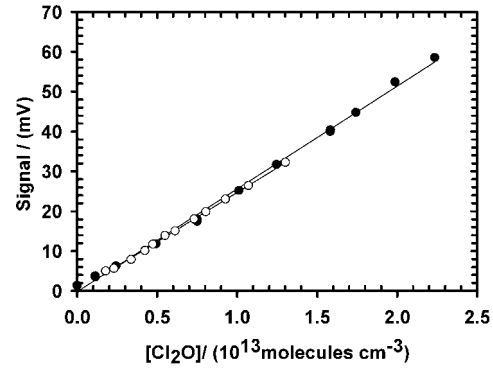

Figure 3. Mass spectrometric calibrations for Cl_2O using both the standard bulb and Br atom titration techniques at 298 K. Filled circles are taken with the standard bulb technique, open circles taken with the titration method.

$$K_{eq(298K)} = 10.1 = \frac{[BrCl]^2}{[Br_2][Cl_2]} \quad (eq2)$$

A calibration curve for BrCl was generated by varying the flow of BrCl through calibrated flow controllers and recording the ion signal from the parent peak of $BrCl^+$ ($m/z = 116$). Figure 3 demonstrates the excellent agreement for Cl_2O calibrations derived using the standard Cl_2O bulb and Br titration techniques. Differences between the two calibration techniques were less than 6% over the full range of experimental temperatures, confirming that decomposition of Cl_2O was negligible in both the standard bulb and the flowmeters.

The mass spectral signal for ClOOCl ($ClOOCl^+$, $m/z = 102$) was calibrated using a slightly modified version of the bromine atom titration scheme described above for Cl_2O.[4] Applied to ClOOCl, titration with atomic bromine results in both BrCl and atomic chlorine. By raising levels of molecular bromine ($\sim 1 \times 10^{13}$ molecules cm^{-3}) in the flow tube relative to those present in the atomic bromine source, we were able to completely convert Cl atoms into BrCl and produce a net result of two BrCl molecules for each reacted ClOOCl.

$$Br + ClOOCl \rightarrow BrCl + ClOO \quad (11)$$

$$ClOO + M \rightarrow Cl + O_2 + M \quad (3)$$

$$\frac{Cl + Br_2 \rightarrow BrCl + Br}{\text{Net: } ClOOCl + Br_2 \rightarrow 2BrCl + O_2} \quad (12)$$

Experimental Results

Reaction Kinetics of OH + Vinyl Bromide. Several experimental runs were conducted for the reaction between vinyl bromide (C_2H_3Br) and hydroxyl radical in order to test our experimental procedure for obtaining reaction rate coefficients. Kinetic measurements were accomplished by monitoring the decay of OH in the presence of excess C_2H_3Br. First-order

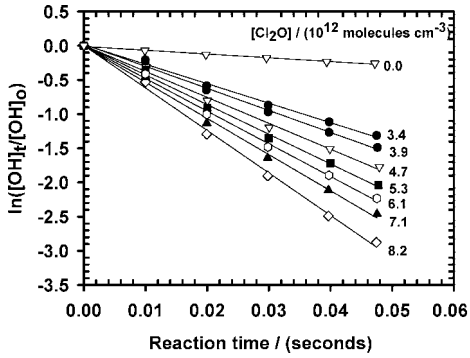

Figure 4. OH decays in the presence of Cl_2O at 298 K.

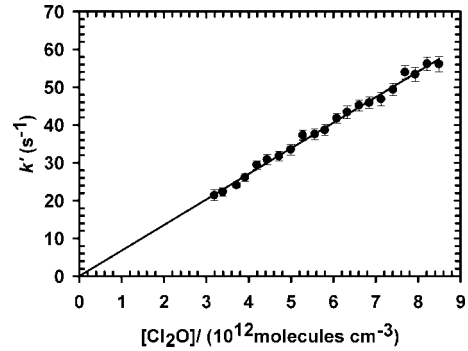

Figure 5. First-order OH decay rates as a function of [Cl_2O] at 298 K.

decays (k') were determined from the slope of the plot of the $\ln([OH]_t/[OH]_o)$ versus reaction time (t) for a given C_2H_3Br concentration where $[OH]_t$ is the number density of OH radical after reaction time t, and $[OH]_o$ defines the initial OH radical concentration.

Vinyl bromide was used in excess ($1-3 \times 10^{12}$ molecules cm^{-3}) over OH radical ($\sim 1 \times 10^{10}$ molecules cm^{-3}), resulting in first-order decays of $6-20$ s^{-1}, similar to what is expected for the kinetic runs for reaction 1. The measured reaction rate constant of $(7.2 \pm 0.5) \times 10^{-12}$ cm^3 $molecule^{-1}$ s^{-1} at 298 K is within 4% of the value reported by Perry et al.[14]

Reaction Kinetics of OH + Cl_2O. Typical OH decays in the presence of Cl_2O are shown in Figure 4. Initial Cl_2O concentrations ranged between 3×10^{12} and 9×10^{12} molecules cm^{-3} over all temperatures. Initial OH concentrations were varied between 0.8×10^{11} and 2×10^{11} molecules cm^{-3}. The resulting first order decays (k') ranged between 20 and 68 s^{-1}. No evidence for nonlinearity in the OH decays was observed over the concentration range used for Cl_2O.

Bimolecular rate coefficients (k_2) were obtained from the weighted linear least-squares fits to the plots of k' versus [Cl_2O]. A typical plot of k' versus [Cl_2O] is shown in Figure 5. The reaction rate coefficient was measured at eleven temperatures between 223 and 303 K. Table 1 contains the measured rate constants as a function of temperature. The temperature dependent data obtained in this study are shown in Figure 6 along with results reported by Stevens et al.,[7] as well as the room temperature results of Ennis et al.[15] and Leu et al.[16] Fitting the rate coefficients measured in this work as a function of temperature to an Arrhenius expression results in the following expression

$$k_6 = (5.1 \pm 1.5) \times 10^{-12} \exp(100 \pm 92/T)\ cm^3\ molecule^{-1}\ s^{-1}$$

where the uncertainties in A and E_a/R are given at the 2σ limit.

TABLE 1: Cl_2O + OH → HOCl + ClO Reaction Rate Coefficients As a Function of Temperature

T (K)	No. of runs	k_6 (10^{-12} cm^3 $molecule^{-1}$ s^{-1})[a]
223	20	8.2 ± 1.3
232	21	8.4 ± 1.2
242	15	7.6 ± 1.2
245	22	7.5 ± 1.1
246	20	6.8 ± 1.0
252	16	7.7 ± 1.1
252	20	7.5 ± 1.1
257	22	7.3 ± 1.1
261	12	8.1 ± 1.2
265	30	8.1 ± 1.2
276	20	7.1 ± 1.1
277	22	7.5 ± 1.1
298	20	7.3 ± 1.1
298	19	7.5 ± 1.1
298	15	6.4 ± 1.0
307	23	7.6 ± 1.1
307	20	6.9 ± 1.0

[a] Uncertainties reported as 2σ.

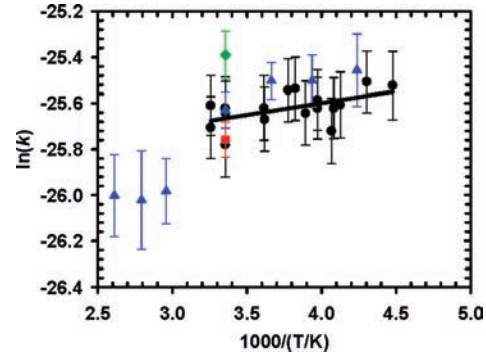

Figure 6. Bimolecular rate constants for OH + Cl_2O as a function of temperature. Solid black circles are the results from this study. Blue triangles are the results of Stevens et al.[7] The green diamond is the 298 K result of Ennis et al.[15] The solid red square is the 298 K result of Leu et al.[16] The solid line is the Arrhenius fit to the results from this work.

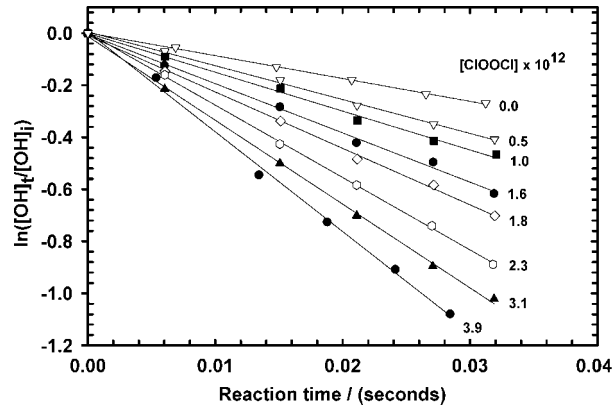

Figure 7. First-order OH decay rates as a function of [ClOOCl] at 298 K.

Reaction Kinetics of OH + ClOOCl. Typical OH decays in the presence of ClOOCl are shown in Figure 7. In addition to correcting for wall loss, the decays were also corrected for the contribution from unreacted Cl_2O using the following expression,

$$k_5[ClOOCl] = k' - k_6[Cl_2O] - k_{wall} \qquad \text{(eq3)}$$

where k_6 is that measured in the current study. Concentrations of Cl_2O were measured at the beginning of each kinetic run.

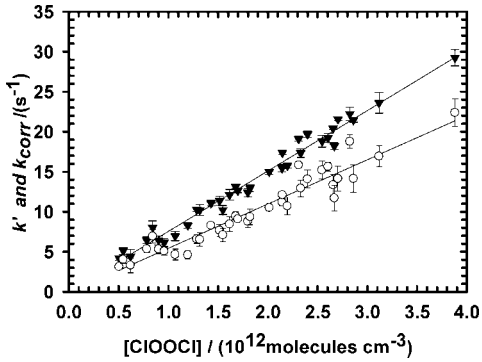

Figure 8. First-order OH decay rates as a function of [ClOOCl] at 298 K. Closed triangles are data without Cl_2O + OH correction. Open circles are data with Cl_2O + OH correction.

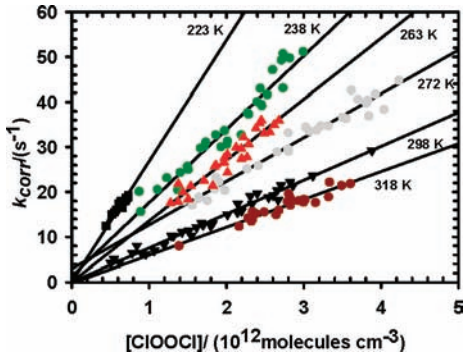

Figure 9. First-order decay rates (k_{corr}) verses [ClOOCl] as a function to temperature. Data is corrected for effects of the OH + Cl_2O reaction.

TABLE 2: ClOOCl + OH → HOCl + ClOO Reaction Rate Coefficients As a Function of Temperature

T (K)	No. of runs	k_5 (10^{-12} cm^3 molecule^{-1} s^{-1})[a]
223	25	13.7 ± 2.4
238	30	9.4 ± 1.8
248	20	8.9 ± 2.1
253	30	7.7 ± 1.6
263	65	7.7 ± 1.7
272	30	7.6 ± 1.4
298	35	6.1 ± 1.2
308	17	5.4 ± 1.2
318	24	5.0 ± 1.6

[a] Uncertainties reported as 2σ.

Corrections for the loss of OH due to the reaction with Cl_2O increased with increasing [ClOOCl]. At the lowest ClOOCl concentrations ($\leq 0.9 \times 10^{12}$ molecules cm^{-3}), the corrections were less than 2%. For moderate ClOOCl concentrations ($(1-2) \times 10^{12}$ molecules cm^{-3}), the corrections decreased k' by 2−6%. At the highest ClOOCl concentrations ($(2.1-4.0) \times 10^{12}$ molecules cm^{-3}), corrections to k' ranged between 6 and 25%. Figure 8 shows the influence of the OH + Cl_2O correction on OH decays measured at 298 K.

Corrected first-order rate constants for reaction 1 between 223−318 K are plotted against [ClOOCl] in Figure 9. As can be observed in the figure, plots of k_{corr} versus [ClOOCl] were linear over the temperature range studied. The rate coefficient was observed to increase with decreasing temperature. Table 2 summarizes the measured rate coefficients as a function of temperature. A fit of the rate coefficient as a function of temperature to an Arrhenius expression is shown in Figure 10. The data in Figure 10 have been corrected for the effect of the

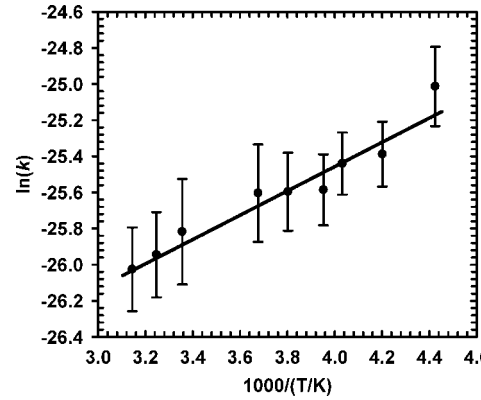

Figure 10. Arrhenius plot for the OH + ClOOCl reaction. E_a/R = 670 ± 230 K.

OH + Cl_2O reaction and wall loss. A weighted least-squares fit to the data in Figure 10 yields the following Arrhenius expression,

$$k_5 = (6.0 \pm 3.5) \times 10^{-13} \exp(670 \pm 230/T) \text{ cm}^3 \text{ molecule}^{-1} \text{ s}^{-1}$$

where the weighting function was of the form $1/\sigma^2$, with σ representing the combination of random and estimated systematic errors.

Unsuccessful attempts were made to observe the products of both reactions 5 and 6. HOCl was not observed due to large background signal at m/z = 52 and 54. ClOO, the anticipated product of reaction 5 was not observed due to its short thermal lifetime[17] and likely extensive fragmentation at the electron energies employed.

Relative Rates for OH + ClOOCl and OH + Cl_2O. As a check on the accuracy of the absolute rate coefficients, we conducted a number of runs at 298 K that measured the relative loss rates of ClOOCl and Cl_2O in the presence of excess OH. Equation 4 describes the decay of ClOOCl and Cl_2O under these conditions.

$$\ln\left\{\frac{[\text{ClOOCl}]_t}{[\text{ClOOCl}]_o}\right\} = \frac{k_1}{k_2} \ln\left\{\frac{[\text{Cl}_2\text{O}]_t}{[\text{Cl}_2\text{O}]_o}\right\} \qquad \text{(eq4)}$$

For these experiments, OH concentrations were increased to between (0.3×10^{13} and 1×10^{13} molecules cm^{-3}. Concentration ratios of [ClOOCl]/[Cl_2O] entering the main reactor were varied between 0.2 and 1.6 by controlling conditions in the ClOOCl prereactor. In the presence of excess OH, simultaneous values of [ClOOCl] and [Cl_2O] were measured at approximately each 5 ms increment of reaction time, up to a total of 40 ms. Figure 11 shows a typical relative rate decay plot corresponding to eq 4. From the slopes of these plots we obtained a value for the ratio of the rate constants of

$$k_5/k_6 = 0.75 \pm 0.15$$

where the uncertainty is at the 2σ limit. This relative rate ratio is in excellent agreement with the value (0.81 ± 0.21) derived from the ratio of absolute rate constants reported above.

In an effort to understand the contribution from secondary chemistry to the observed k_5/k_6 ratios, a kinetic model containing reactions 5, 6, 3, 8 as well as reactions for OH + ClO, OH + HOCl, and OH + HCl was used. The model was used in conjunction with the concentrations of ClOOCl and Cl_2O found in Table 3. As a consequence of the chlorine atoms liberated from reaction 5, the model predicts that the observed k_5/k_6 ratio should be larger than the expected ratio calculated by ratioing the absolute rate constants, by between 3 and 8%.

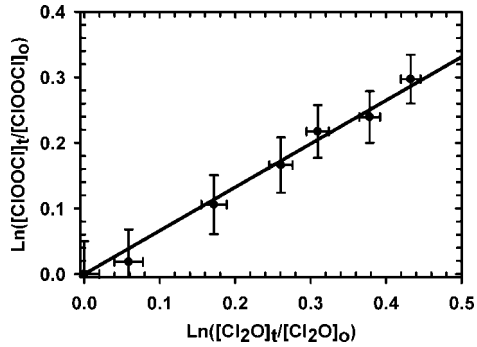

Figure 11. Typical relative rate decay for OH + ClOOCl using OH + Cl_2O as the reference reaction.

TABLE 3: Relative Rate Determinations for Reactions 5 and 6 under excess OH conditions at 298 K

run	[ClOOCl]/[Cl_2O] (10^{12} molecules cm^{-3})	k_5/k_6[a]	modeled k_5/k_6
1	1.3/1.2	0.88 ± 0.04	0.91
2	2.0/5.2	0.77 ± 0.04	0.94
3	2.0/6.7	0.86 ± 0.07	0.94
4	1.7/6.7	0.70 ± 0.04	0.94
5	1.6/6.7	0.70 ± 0.03	0.95
6	1.6/6.8	0.77 ± 0.05	0.95
7	1.3/7.9	0.68 ± 0.06	0.94
8	1.3/5.4	0.75 ± 0.05	0.95
9	1.8/1.2	0.63 ± 0.04	0.95
10	1.8/1.2	0.71 ± 0.04	0.95
11	1.8/1.1	0.82 ± 0.1	0.91
12	1.7/1.1	0.72 ± 0.06	0.91

[a] Uncertainties reported as 2σ.

The influence of the secondary reaction between OH + ClO, through its branch producing Cl and HO_2, is another source of ClOOCl and Cl_2O loss. The largest contribution from secondary chemistry, at the ~10% level, is predicted to occur when the ratio of [ClOOCl]/[Cl_2O] is the smallest. This is due to the enhanced rate of Cl_2O loss, relative to ClOOCl, and the resulting increase in chlorine atom production from the reaction of OH + ClO. However, this difference could not be discerned within the scatter of the measured ratios.

Ab Initio Calculations

Computational Method. To gain insight into the structures and resulting potential energy surface of the OH + ClOOCl reaction, ab initio calculations were carried out using the Gaussian 98 and Gaussian 03 suite of programs.[18] Optimizations were performed using the hybrid density MPW1K method and basis sets that ranged from 6−311++G(d,p) to 6−311++G(3df,3pd). Geometries were optimized using Schlegel's method to better than 0.001 Å for bond lengths and 0.01° for bond angles, with a self-consistent field convergence of at least 10^{-6} on the density matrix. The residual force was less than 10^{-4} atomic units. The expectation value $<s^2>$ was monitored for all species. The expectation value never exceeded 0.78, before spin-annihilation, for any of the open shell species, namely the ClOOCl−OH transition state (ClOOCl−$OH^{\ddagger}$), the ClOOCl-OH prereactive complex (ClOOCl−$OH_{complex}$), and ClOO. This indicates that the wavefunction is not contaminated by higher multiplicity states.

Performing a frequency calculation tested the positions of the resulting geometries on the potential energy surface. All species except for the transition state were found to have only positive frequencies, confirming that they were minima on the PES. One imaginary frequency was found for the transition state structure, verifying its position as a maximum in one coordinate and a minimum in all other coordinates. Intrinsic reaction coordinate (IRC) calculations were performed on the transition state in both the forward and reverse directions. The IRC calculations connected the prereactive complex and reaction products to the calculated transition state.

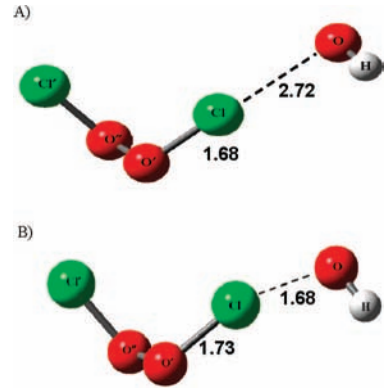

Figure 12. Optimized structures for the prereactive complex (A) and transition state (B) for the OH + ClOOCl reaction as calculated at the MPW1K/6−311++G(3df,3pd) level. Bond lengths are in Ångströms.

Single-point calculations were performed on all species using the optimized geometries found at the MPW1K/6−311++G(3df,3pd) level. These calculations were performed using the CCSD(T) method coupled with the 6−31G(d,p), 6−31G(2d,2p), 6−311++G(2df,2pd), and 6−311++G(3df,3pd) basis sets. Zero-point energies and harmonic vibrational frequencies were calculated at the MPW1K/6−311++G(3df,3pd) level using the optimized geometries determined with the same method/basis set combination.

Computational Results. Optimized geometries and absolute and relative energies for ClOOCl, OH, ClOOCl−$OH_{complex}$, ClOOCl−$OH^{\ddagger}$, ClOO, and HOCl were determined as a function of method and basis set and are shown in Tables S1 and S2 of the Supporting Information. The calculated vibrational frequencies for all species at the MPW1K/6−311++G(3df,3pd) level are shown in Table S3 of the Supporting Information. Shown in Figure 12 are the optimized geometries found at the MPW1K/6−311++G(3df,3pd) level for ClOOCl−$OH_{complex}$ and ClOOCl−$OH^{\ddagger}$ (transition state). The optimized geometries are in excellent agreement with those reported from microwave spectroscopy studies of ClOOCl.[19] For instance, the Cl−O′ (1.68 Å) and O′−O″ (1.36 Å) bond lengths calculated at the MPW1K/6−311++G(3df,3pd) level compare well with the measured values of 1.70 Å and 1.43 Å, respectively. Similarly, the calculated bond angles for ClO′O″ and the Cl′O″O′Cl dihedral are within a few degrees of the experimentally measured angles.

On the basis of the calculated geometries, we have constructed a potential energy surface for the OH + ClOOCl reaction, using energy values found at the CCSD(T)/6−311++G(3df,3pd) level without zero-point energy correction (Figure 13). The minimum energy path to products is found to proceed through a prereactive complex, which is calculated to be bound by 2.61 kcal mol^{-1} relative to the reactants. The prereactive complex is characterized by a very loose interaction between the terminal Cl and the incoming hydroxyl oxygen atom. In addition, there is virtually no change in the length of the internal dimer O−Cl bond that is adjacent to the newly formed dimer chlorine−hydroxyl oxygen bond.

As the reaction progresses through the transition state the newly formed Cl−O bond length decreases dramatically (2.72

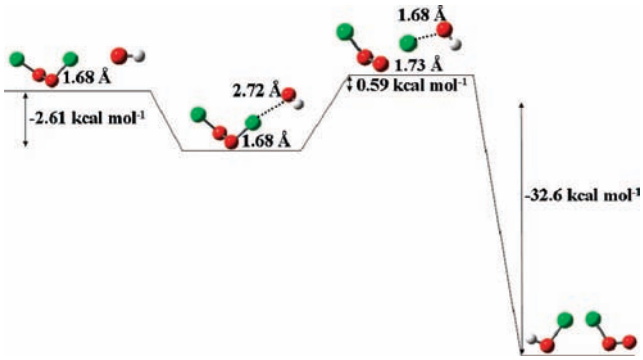

Figure 13. Potential energy surface for the OH + ClOOCl reaction. Bond lengths are in angstroms and are calculated at the MPW1K/6−311++G(3df,3pd) level. Energies are in kcal mol^{-1} and are calculated at the QCISD(T)/6−311++G(2d,2p) level.

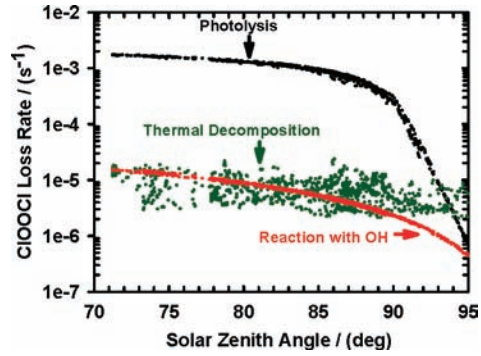

Figure 14. Loss rates for ClOOCl in units of s^{-1} calculated using the Caltech/JPL atmospheric model. Model inputs are discussed in the text.

Å → 1.68 Å) along with a small (3%) increase in the dimer O−Cl bond length. The transition state energy is calculated to be ∼0.6 kcal mol^{-1} above the energy of the reactants and the activation barrier is not distinguishable from zero within the uncertainty of the calculations. Exiting from the transition state leads to the breaking of the internal dimer Cl−O bond and formation of a new O−Cl bond to produce HOCl and ClOO. The overall reaction enthalpy is calculated to be −32.6 kcal mol^{-1} at 0 K, which compares favorably with the NASA recommended value of −33.9 ± 1.3 kcal mol^{-1} at 298 K.[2]

The existence of an intermediate complex, as suggested by the ab initio calculations, is consistent with the experimentally determined negative temperature dependence, which arises from the competition between product formation and reactant reformation during dissociation of the intermediate. In this case, decreasing the temperature increasingly favors the formation of products that may be due to the higher density of states along this pathway. An ab initio dynamics study of this potential including a calculation of the density of states would offer addition insights on the effect of the prereactive complex on the temperature dependence of this reaction. This would allow for comparison of the observed versus calculated temperature dependence.

Discussion

This study reports the first experimental measurements and computational studies of the kinetics and mechanism of the OH + ClOOCl reaction. The ab initio calculations indicate that the reaction involves chlorine abstraction by OH and proceeds through a weakly bound complex. Our measurement of a relatively small *A*-factor (6.0×10^{-13} cm^3 molecule^{-1} s^{-1}) and negative activation energy (−0.67 kcal/mol) is consistent with the ab initio calculations, which indicate that the mechanism involves a weakly bound intermediate. This mechanism is further supported by our measurements of similar kinetic parameters for the OH + Cl_2O reaction, which likely proceeds via an analogous mechanism.

Rate constant data measured in this study for the OH + Cl_2O reaction are in excellent agreement with the results reported by Stevens et al.[7] over the temperature range of our study (223−307 K), as well as with the room temperature values of Leu et al.[16] and Ennis et al.[15] Stevens et al.[7] also report rate constant values outside the temperature range of the current experiment (i.e., 307−383 K) that are significantly smaller than the values obtained by extrapolating our data to the higher temperatures. As a possible explanation for this discrepancy, we note that previous work in our laboratory has indicated that Cl_2O can be lost via surface-catalyzed thermal decomposition. Stevens et al.[7] in their investigation of the OH + Cl_2O reaction reported significant curvature in the pseudo first-order decays measured at high temperatures and long reaction times that were independent of the initial OH concentration. We suggest that the curvature in the pseudo first-order plots could be due to thermal decomposition of Cl_2O on the flow tube wall and that a linear fit of these curved plots over the entire reaction time would impart a low bias to the first-order decay constants.

Stevens et al. also found that the OH + Cl_2O reaction exhibits a strong pressure dependence, with the rate constant increasing nearly 25% between 1 and 4 Torr. Although the present experimental results provide no further insight on this pressure dependence, the ab initio calculations suggest that such a strong pressure dependence is unlikely for ClOOCl given the small binding energy of the prereactive complex.

Atmospheric Significance. As discussed above, the OH + ClOOCl reaction is the rate-limiting step in a polar catalytic ozone destruction cycle coupling the HO_x and ClO_x radical families. The importance of this reaction depends largely on the degree to which its catalytic cycle competes with the cycle involving ClOOCl photolysis as the rate-limiting step. Figure 14 shows the loss rates (s^{-1}) for ClOOCl from the OH + ClOOCl and ClOOCl photolysis calculated by the JPL/Caltech stratospheric model under Arctic stratospheric conditions encountered during the joint SOLVE/THESEO-2000 aircraft mission of winter 1999/2000.[20] A more thorough description of the conditions sampled during this campaign can be found in Newman et al.[20] and in the references contained therein. For these calculations, concentration values for ClO_x were taken from the aircraft observations along the flight track, whereas OH concentrations were specified as a function of solar zenith angle using a formula derived from in situ measurements of OH during the SOLVE/THESEO-2000 mission.[21] The photolysis loss rate (*J*) values were calculated by inputting the NASA-recommended ClOOCl absorption cross sections into a radiative transfer model constrained by maps of ozone reconstructed using measurements from the Polar Ozone Aerosol Measurement satellite instrument.[22] Figure 14 also shows the first-order loss of ClOOCl from thermal decomposition, calculated using laboratory data from Nickolaisen et al.[23] extrapolated to the appropriate atmospheric temperatures.

The model calculations indicate that during sunlight hours (solar zenith angle, SZA < 90°) photolysis is the primary removal mechanism for ClOOCl, with thermal decomposition and reaction with OH each accounting for only 0.5−1% of the loss. During twilight conditions (90° < SZA < 95°), photolytic removal rates decrease much more rapidly than the rates for

thermal decomposition and reaction with OH. At SZA = 93°, for instance, where the overall loss rate drops to 1% of the daylight rate, reaction with OH contributes approximately 15% to the loss of ClOOCl. On the basis of these calculations, we conclude that the overall effect of including the OH + ClOOCl reaction is to slightly increase (~1%) the calculated amount of Arctic ozone destruction.

The ClOOCl cross sections from Pope et al. result in *J* values that are about a factor of 6 smaller than those shown in Figure 14. Use of these cross sections in the model will increase the importance of the OH + ClOOCl cycle relative to the ClOOCl photolysis cycle by approximately the same factor. However, this comparison is not particularly meaningful because the much lower ClOOCl photolysis rates result in a failure of the model to reproduce the observed springtime ozone depletion observed in the polar regions. This discrepancy highlights the need for additional laboratory studies on catalytic ozone destruction mechanisms in the polar stratosphere.

Acknowledgment. The authors gratefully acknowledge the technical assistance of Dave Natzic, and valuable discussions with Trevor Ingham and Kyle Bayes, and the modeling work of Ross Salawitch. We thank Kyle Bayes for his critical reading of the manuscript. The research described in this paper was carried out at the Jet Propulsion Laboratory, California Institute of Technology, under contract to the National Aeronautics and Space Administration. This work was supported by the NASA Upper Atmosphere Research and Tropospheric Chemistry Programs.

Supporting Information Available: Supplementary tables as described in the text are provided. This material is available free of charge via the Internet at http://pubs.acs.org.

References and Notes

(1) Stimpfle, R. M. , Wilmouth, D. M.; Salawitch, R. J.; Anderson, J. G. , *J. Geophys. Res.-Atmos.* **2004**, *109*, 003301.

(2) Sander, S. P.; Finlayson-Pitts, B. J.; Friedl, R. R.; Golden, D. M.; Huie, R. E.; Kolb, C. E.; Kurylo, M. J.; Molina, M. J.; Moortgat, G. K.; Orkin, V. L.; Ravishankara, A. R. *Chemical Kinetics and Photochemical Data for Use in Atmospheric Studies*, Evaluation Number 14; Jet Propulsion Laboratory, **2002**.

(3) Pope, F. D.; Hansen, J. C.; Bayes, K. D.; Friedl, R. R.; Sander, S. P. , *J. Phys. Chem. A* **2007**, In press.

(4) Ingham, T.; Sander, S. P.; Friedl, R. R. *Faraday Discuss.* **2005**, *130*, 89.

(5) Cox, R. A.; Hayman, G. D. *Nature* **1988**, *332*, 796.

(6) Cox, R. A.; Derwent, R. G.; Eggleton, A. E. J.; Read, H. J. *J. Chem. Soc. Faraday Trans. I* **1979**, *75*, 1648.

(7) Stevens, P. S.; Anderson, J. G. *J. Phys. Chem.* **1992**, *96*, 1708.

(8) Marrero, T. R.; Mason, E. A. *J. Phys. Chem. Ref. Data* **1972**, *1*, 3.

(9) Sander, S. P.; Watson, R. T. *J. Phys. Chem.* **1980**, *84*, 1664.

(10) Friedl, R. R.; Sander, S. P. *J. Phys. Chem.* **1989**, *93*, 4756.

(11) Knauth, H. D.; Alberti, H.; Clausen, H. *J. Phys. Chem.* **1979**, *83*, 1604.

(12) Maric, D.; Burrows, J. P.; Meller, R.; Moortgat, G. K. *J. Photochem. Photobiol., A* **1993**, *70*, 205.

(13) Maric, D.; Burrows, J. P.; Moortgat, G. K. *J. Photochem. Photobiol., A* **1994**, *83*, 179.

(14) Perry, R. A.; Atkinson, R.; Pitts, J. N. *J. Chem. Phys.* **1977**, *67*, 458.

(15) Ennis, C. A.; Birks, J. W. *J. Phys. Chem.* **1988**, *92*, 1119.

(16) Leu, M. T.; Lin, C. L. *Geophys. Res. Lett.* **1979**, *6*, 425.

(17) Zhu, R. S.; Lin, M. C. *J. Chem. Phys.* **2003**, *119*, 2075.

(18) Frisch, M. J. T. G. W.; Schlegel, H. B.; ScuseriaG. E.; Robb, M. A.; Cheeseman, J. R.; Zakrzewski, V. G. , Montgomery, J. A. Jr. ; Stratmann, R. E. , Burant, J. C. , Dapprich, S.; Millam, J. M.; Daniels, A. D.; Kudin, K. N.; Strain, M. C.; Farkas, O.; Tomasi, J.; Barone, V.; Cossi, M.; Cammi, R.; Mennucci, B.; Pomelli, C.; Adamo, C.; Clifford, S.; Ochterski, J.; Petersson, G. A.; Ayala, P. Y.; Cui, Q.; Morokuma, K.; Malick, D. K. , Rabuck, A. D.; Raghavachari, K.; Foresman, J. B.; Cioslowski, J.; Ortiz, J. V.; Stefanov, B. B.; Liu, G.; Liashenko, A.; Piskorz, P.; Komaromi, I.; Gomperts, R.; Martin, R. L.; Fox, D. J.; Keith, T.; Al-Laham, M. A.; Peng, C. Y.; Nanayakkara, A.; Gonzalez, C.; Challacombe, M.; Gill, P. M. W.; Johnson, B. G.; Chen, W.; Wong, M. W.; Andres, J. L.; Head-Gordon, M.; Replogle, E. S.; Pople, J. A. *Gaussian, Inc* 1998.

(19) Birk, M.; Friedl, R. R.; Cohen, E. A.; Pickett, H. M.; Sander, S. P. *J. Chem. Phys.* **1989**, *91*, 6588.

(20) Newman, P. A.; Harris, N. R. P.; Adriani, A.; Amanatidis, G. T.; Anderson, J. G.; Braathen, G. O.; Brune, W. H.; Carslaw, K. S.; Craig, M. S.; DeCola, P. L.; Guirlet, M.; Hipskind, R. S.; Kurylo, M. J.; Kullmann, H.; Larsen, N.; Megie, G. J.; Pommereau, J. P.; Poole, L. R.; Schoeberl, M. R.; Stroh, F.; Toon, O. B.; Trepte, C. R.; Van Roozendael, M. , *J. Geophys. Res.-Atmos.* **2002**, *107*, 8259.

(21) Hanisco, T. F.; Smith, J. B.; Stimpfle, R. M.; Wilmouth, D. M.; Anderson, J. G.; Richard, E. C.; Bui, T. P. *J. Geophys. Res.-Atmos.* **2002**, *107*, 8283.

(22) Salawitch, R. J.; Wofsy, S. C.; Wennberg, P. O.; Cohen, R. C.; Anderson, J. G.; Fahey, D. W.; Gao, R. S.; Keim, E. R.; Woodbridge, E. L.; Stimpfle, R. M.; Koplow, J. P.; Kohn, D. W.; Webster, C. R.; May, R. D.; Pfister, L.; Gottlieb, E. W.; Michelsen, H. A.; Yue, G. K.; Wilson, J. C.; Brock, C. A.; Jonsson, H. H.; Dye, J. E.; Baumgardner, D.; Proffitt, M. H.; Loewenstein, M.; Podolske, J. R.; Elkins, J. W.; Dutton, G. S.; Hintsa, E. J.; Dessler, A. E.; Weinstock, E. M.; Kelly, K. K.; Boering, K. A.; Daube, B. C.; Chan, K. R.; Bowen, S. W. *Geophys. Res. Lett.* **1994**, *21*, 2547.

(23) Nickolaisen, S. L.; Friedl, R. R.; Sander, S. P. *J. Phys. Chem.* **1994**, *98*, 155.

JP8007706